

Article

Structural Disorder in High-Spin $\{\text{Co}^{\text{II}}_9\text{W}^{\text{V}}_6\}$ (Core)-[Pyridine N-Oxides] (Shell) Architectures

Michał Liberka , Jędrzej Kobylarczyk  and Robert Podgajny * 

Faculty of Chemistry, Jagiellonian University in Kraków, Gronostajowa 2, 30-387 Kraków, Poland; michal.liberka@gmail.com (M.L.); jedrzej.kobylarczyk@uj.edu.pl (J.K.)

* Correspondence: robert.podgajny@uj.edu.pl; Tel.: +48-12-686-2459

Academic Editor: Takashiro Akitsu

Received: 18 December 2019; Accepted: 6 January 2020; Published: 8 January 2020



Abstract: The combinations of Co(II), octacyanidotungstate(V), and monodentate pyridine *N*-oxide (pyNO) or 4-phenylpyridine *N*-oxide (4-phpyNO) led to crystallization of novel crystalline phases $\{\text{Co}^{\text{II}}[\text{Co}^{\text{II}}_8(\text{pyNO})_{12}(\text{MeOH})_{12}][\text{W}^{\text{V}}(\text{CN})_8]_6\}$ (**1**) and $\{\text{Co}^{\text{II}}[\text{Co}^{\text{II}}_8(4\text{-phpyNO})_7(\text{MeOH})_{17}][\text{W}^{\text{V}}(\text{CN})_8]_6\} \cdot 7\text{MeOH} \cdot (4\text{-phpyNO})_3$ (**2**). In both architectures, metal–cyanide clusters are coordinated by *N*-oxide ligands in a simple monodentate manner to give the spherical objects of over 1 nm core diameter and about 2.2 nm (**1**) and 3 nm (**2**) of the total diameter, terminated with the aromatic rings. The supramolecular architecture is dominated by dense and rich π – π interaction systems. Both structures are characterized by a significant structural disorder in ligand shell, described with the suitable probability models. For **1**, the π – π interactions between the pyNO ligands attached to the same metal centers are suggested for the first time. In **2**, 4-phpyNO acts as monodentate ligand and as the crystallization molecule. Magnetic studies indicate the high-spin ground state due to the ferromagnetic interactions Co(II)–W(V) through the cyanido bridges. Due to the high symmetry of the clusters, no signature of slow magnetic relaxation was observed. The characterization is completed by solid-state IR and UV–Vis–NIR spectroscopy. The conditions for the stable $\text{M}_9\text{M}'_6$ -based crystals formation are synthetically discussed in terms of the type of capping ligands: monodentate, bridging, and chelating. The potential of the related polynuclear forms toward the magnetism-based functional properties is critically indicated.

Keywords: magnetic coordination materials; crystal engineering; polynuclear clusters; surface decoration; molecular disorder; octacyanidometalates

1. Introduction

Cyanido-bridged 0D systems of the various linear, polygon, or cluster topologies and 1D chains or ribbons were recently presented in searching for molecular platforms suitable for single-molecule magnet functions. The critical underlying prerequisite—axial magnetic anisotropy—has been shaped through cyanide-bridging of suitable d and f metal ion and dedicated coordination surrounding. For example, among the frequently exploited building blocks, one can indicate 6-coordinated *fac*- $[\text{M}(\text{L})(\text{CN})_3]^-$ ($\text{M} = \text{Fe}^{\text{III/II}}, \text{Co}^{\text{III/II}}$; *L*-hydrotris(pyrazol-1-yl)borate, tetra(pyrazol-1-yl)borate moieties with trigonal distortion [1–4], octahedral Co^{II} with axial deformation [5,6], *trans*- $[\text{M}(\text{L})(\text{CN})_2]$ ($\text{M} = \text{Fe}, \text{Cr}$; *L*-planar pentadentate ligands) heptagonal bipyramidal moieties [7,8] or intrinsically anisotropic 4d or 5d heavy metal precursors [9], and lanthanide complexes [10,11].

Along this line, investigation of the crystalline phases composed of six capped body-centered cube $\text{Co}_9\text{M}'_6$ clusters as molecular platforms for magnetic relaxations suggests the following image of structure–properties correlations. Twelve compounds were studied structurally and magnetically, counting the original $\{\text{Co}_9\text{M}_6(\text{MeOH})_{24}\} \cdot \text{solv}$ ($\text{M} = \text{Mo}, \text{W}$) phases [12] and those equipped with various ligands: chelating, 2,2'-bipyridine-*N*-oxide (2,2'-bpno) [13], 2,2'-bipyridine-*N,N'*-dioxide

(2,2'-bpdo) [14], and methylpyridinemethanol (mpm) [15], as well as bridging 4,4'-bipyridine-*N*-oxide (4,4'-bpmo) [16], 4,4'-bipyridine-*N,N'*-dioxide (4,4'-bpdo) [17], and pyrazine-*N*-oxide (pzmo) [16]. The unequivocal direct fitting of $\ln\tau(T^{-1})$ point set using the Arrhenius law was possible only in the case $\{\text{Co}_9\text{W}_6(2,2'\text{-bpdo})_6(\text{MeOH})_{12}\}\{\text{Co}_9\text{W}_6(2,2'\text{-bpdo})_7(\text{MeOH})_{10}\}\cdot 8\text{H}_2\text{O}\cdot 2\text{MeCN}\cdot 27\text{MeOH}$ to give the best $\Delta E/k_B$ of 30.0(8) K along the whole series [14]. Interestingly, the Cole–Cole plot indicated that only half of the clusters took part in the relaxation process. The relaxation behavior was then assigned solely to the $\text{Co}_9\text{W}_6(2,2'\text{-bpdo})_7(\text{MeOH})_{10}$ cluster with only one external Co site free of chelating ligand, and related to the sufficient axial character of the cluster core. No correlation was found between the magnetic ac data and the intercluster distance, quality of intercluster contacts, or composition of the first coordination sphere.

The inherent issue along the above series was the tuning of the extent of cluster coverage, size, shape, and quality of the peripheral regions resulting from the molecular structure and coordination modes of external ligands. The bis-chelating diimine-*N*-oxide and other related ligands increase the hydrophobic character of the external regions and set the average diameter between 1.9 and 2.2 nm, compared to the diameter of 1.6 nm for non-chelated $\{\text{Co}_9\text{W}_6(\text{MeOH})_{24}\}$. On the contrary, ditopic 4,4'-bridging congeners provides the star-like branched coordination backbones (discrete or chain-like) with molecular diameters between ca. 2.1 and 2.7 nm with the remote hydrophilic functions exposed at the peripheral parts. Such forms tend to create polymeric forms; however, they can be also expected to bind the external remote functional coordination units. In general, the variety of multifaceted intercluster supramolecular synthons were observed in the related crystal structures, and rather without the straightforward correlation between the ligand type and related intercluster separation.

Having in mind the above experiences with the Co_9W_6 cluster family, we performed the decoration of the Co_9W_6 core with the monodentate pyridine *N*-oxide (pyNO) or 4-phenylpyridine *N*-oxide (4-phpyNO), which provides the singly and presumably less tightly bonded hydrophobic ends of pyridine and phenyl group. Driven by curiosity, we aimed to test the new type of ligands for alternative coordination modes and supramolecular organization toward (rather a serendipitous) occurrence of a higher degree of magneto-structural asymmetry that allows unblocking the slow magnetic relaxations. We present the crystal structures, spectroscopic characterization, and magnetic properties of new $\{\text{Co}^{\text{II}}[\text{Co}^{\text{II}}_8(\text{pyNO})_{12}(\text{MeOH})_{12}][\text{W}^{\text{V}}(\text{CN})_8]_6\}$ (1) and $\{\text{Co}^{\text{II}}[\text{Co}^{\text{II}}_8(4\text{-phpyNO})_7(\text{MeOH})_{17}][\text{W}^{\text{V}}(\text{CN})_8]_6\}\cdot 7\text{MeOH}\cdot (4\text{-phpyNO})_3$ (2) congener.

2. Results and Discussion

2.1. Structural Studies

Both new compounds **1** and **2** were obtained in crystalline form. All samples were characterized by IR and UV–Vis spectra, TGA, and CHN elemental analysis (Figures S1–S3, ESI⁺) followed by a single-crystal X-ray diffraction analysis (Figure 1, Table 1, and Figures S4–S8, Tables S1 and S2, ESI⁺). The symmetrically independent parts are presented in Figures S4 and S5 (ESI⁺). The results of data collection and structure refinement have been summarized in Table 1. Compounds **1** and **2** crystallize in the trigonal $R\bar{3}$ and triclinic $P\bar{1}$ crystallographic space group, respectively. The crystal structures of both compounds consist of pentadecanuclear cyanide-bridged clusters $\{\text{Co}_9\text{W}_6\text{L}_x(\text{MeOH})_{24-x}\}$ (Figure 1) due to the cluster surface decoration with monodentate pyridine *N*-oxide (pyNO, L^1 , $x = 12$) for **1** or 4-phenylpyridine *N*-oxide (4-phpyNO, L^2 , $x = 7$) for **2**. The cluster core in both cases is analogous to the six capped body-centered cubes of broad $\text{M}_9\text{M}'_6$ family. In both cases, the central $[\text{Co}(\mu\text{-NC})_6]^{2+}$ moiety with almost perfect octahedron geometry (Tables S3 and S4, ESI⁺) is surrounded by six cyanide-bridges directed toward six $[\text{W}(\mu\text{-CN})_5(\text{CN})_3]^{3-}$ blocks located in the vertices of super-octahedron. The eight remaining Co^{2+} ions are located in the corners of the super-cube, each accepting three cyanide-bridges from the neighboring W centers, reaching the general composition $\text{fac-}[\text{Co}^{\text{II}}(\mu\text{-NC})_3\text{L}_y(\text{MeOH})_{3-y}]^-$. In compound **1**, two crystallographically independent external $\text{fac-}[\text{Co}_{2/3}(\mu\text{-NC})_3(\text{pyNO})_{1.5}(\text{MeOH})_{1.5}]^{2+}$ moieties are

distinguished, with occupancy 0.25, 0.5, 0.75, or 1.0 of the organic and solvent ligands (see Figure S4, ESI†). In compound **2**, four crystallographically independent external cobalt moieties were found: one $\text{fac}[\text{Co}_3(\mu\text{-NC})_3(\text{MeOH})_3]^{2+}$, two $\text{fac}[\text{Co}_2/5(\mu\text{-NC})_3(4\text{-phpyNO})(\text{MeOH})_2]^{2+}$, and one $\text{fac}[\text{Co}_4(\mu\text{-NC})_3(4\text{-phpyNO})_{1.5}(\text{MeOH})_{1.5}]^{2+}$ (with occupancy 0.5 or 1.0 of the organic and solvent ligands, see Figure S5, ESI†). All Co^{2+} ions exhibit practically O_h geometry (Tables S3 and S4, ESI†). The Co-N/O distances in **1** and **2** are in the range of 2.061–2.123 Å, which is typical for Co_9W_6 -based clusters with monodentate ligands. All $[\text{W}(\mu\text{-CN})_5(\text{CN})_3]^{3-}$ ions connect five cobalt ions, while three cyanide ligands are terminal. Chosen distances and angles are collected in Tables S1 and S2 (ESI†). All values are in line with the related literature data [13–17].

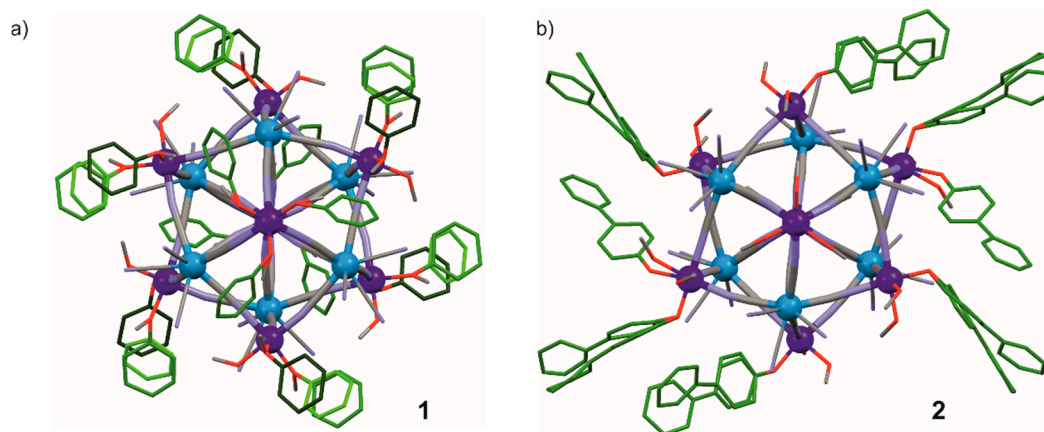


Figure 1. Pentadecanuclear clusters in the crystal structure of **1** (a) and **2** (b). Hydrogens atom, crystallization solvents, and non-coordinated ligands were omitted for clarity. Legend: Co—navy blue; W—light blue; C—dark gray; N—violet; O—red; C and N in pyNO and 4-pphyNO ligands—dark green (75% occupancy), green (50% occupancy), and light green (25% occupancy) (for details see Supplementary Materials).

The application of a new type of ligands to fifteen-centered clusters allowed obtaining a completely new character of the ligand shell. In **1**, pyNO ligands connected to the Co_3 moieties interacts with each other with π - π interactions, which has not been seen in $\text{M}_9\text{M}'_6\text{L}_x$ clusters with monodentate coordination of ambidentate linkers (L = pyrazine mono-*N*-oxide (pzmo)) and 4,4'-bipyridine mono-*N*-oxide (4,4'-bpdo, Figure S6, ESI†) [16]. Supramolecular arrangement is also dominated by this type of interaction, but there are also weak $\text{O}_3\text{MeOH}\cdots\text{N}_8\text{CN}$ hydrogen bonds in the direction [001]. Each cluster is surrounded symmetrically by six other clusters, creating a densely packed 3D supramolecular architecture. The shortest intercluster distance is 5.22 Å, which conforms to the absence of additional solvent molecules in the molecular architecture. No interactions between 4-pphyNO ligands coordinated to the same metallic center are observed in the case of **2**, which is in line with a relatively large freedom of rotation of the phenyl ring. The crystal structure of **2** is completed with additional crystallization MeOH molecules, creating a network of hydrogen bond synthons, as well as uncoordinated 4-pphyNO molecules (with occupancy 0.5 or 1.0; Figure S6, ESI†). The face-to-face or edge-to-face π - π interactions between coordinated and uncoordinated ligands form supramolecular layers perpendicular to the [010] direction, which are additionally stabilized by $\text{O}_5\text{MeOH}\cdots\text{N}_3\text{CN}$ hydrogen bonds. Longer ligand and also the presence of uncoordinated 4-pphyNO molecules in **2** compared to **1** result in the larger separation of clusters. The shortest distance between them is 7.23 Å, and the clusters are not distributed in such a symmetrical manner as in the case of **1**. The structural uniformity has been confirmed using powder X-ray diffraction data (Figure S9, ESI†).

Table 1. Crystal data and structure refinement for 1 and 2.

Compound	1	2
Formula	Co ₉ W ₆ C ₁₂₀ H ₁₀₈ N ₆₀ O ₂₄	Co ₉ W ₆ C ₁₈₃ H ₁₅₉ N ₅₈ O ₃₄
Formula weight/g·mol ⁻¹	4408.04	5348.14
T/K	100	100
λ/Å	0.71073	0.71073
Crystal system	Trigonal	Triclinic
Space group	R $\bar{3}$	P $\bar{1}$
Unit cell		
a/Å	28.126(4)	17.179(1)
b/Å	28.126(4)	17.513(1)
c/Å	18.038(2)	20.029(1)
α/deg	90	83.770(1)
β/deg	90	79.935(1)
γ/deg	120	64.080(1)
V/Å ³	12,358.0(30)	5333.1(4)
Z	3	1
Calculated density/g·cm ⁻³	1.777	1.665
Absorption coefficient/cm ⁻¹	5.125	3.978
F(000)	6381	2622
Crystal size/mm × mm × mm	0.41 × 0.27 × 0.18	0.33 × 0.27 × 0.21
θ range/deg	2.48 to 25.38	2.30 to 25.39
Limiting indices	-33 < h < 33 -33 < k < 29 -21 < l < 21	-20 < h < 20 -20 < k < 20 -23 < l < 23
Collected reflections	5210	9900
Symmetry independent reflections	4818	18,710
R _{int}	0.1055	0.0372
Completeness/%	99.0	99.3
Data/restraints/parameters	4818/463/472	18710/926/1856
GOF on F ²	1.093	1.394
Final R indices	R[F ² > 2σ(F ²)] = 0.0675 wR(F ²) = 0.1564	R[F ² > 2σ(F ²)] = 0.0804 wR(F ²) = 0.1740
Largest diff peak and hole/e·Å ³	1.851/-1.759	1.409/-2.372

To discuss the above structural description, we consider below the observations for the entire M₉M'₆L_x family of compounds, focusing on (i) the molar ratios in the parent solution and in the final product, and (ii) on the structural disorder in the ligand shell. All previous reports on functionalized fifteen-centered cluster cores were associated with O,O-, N,O-, N,N-, or N,N,N-donor ligands providing their monodentate (**m**), bidentate (**b**), or tridentate (**t**) local coordination: Mn₉W₆L_x (L = 4,4'-bipyridine, x = 4, **m**; *trans*-1,2-di(4-pyridyl)ethylene, x = 5, **m**; 4,4'-dipyridyl disulfide, x = 4, **m**; 4,4'-di-*tert*-butyl-2,2'-bipyridine, x = 8, **b**; 4,7-di-phenyl-1,10-phenantroline, x = 8, (**b**), Fe₉M'₆(Me₃tacn)₈ (Me₃tacn = 1,4,7-trimethyl-1,4,7-triazacyclononane; M' = W, Re, **t**), Co₉W₆L_x (L = 4,4'-bipyridine di-*N*-oxide, x = 12, **m**; (R/S)methylpyridinemethanol, x = 8, **b**; 2,2'-bipyridine di-*N,N*-oxide, x = 6/7, **b**; 2,2'-bipyridine mono-*N*-oxide, x = 6 or 8 **b**; 4,4'-bipyridine mono-*N*-oxide, x = 4 or 6, **m**; pyrazine mono-*N*-oxide, x = 5, **m**), Ni₉W₆L_x (L = 2,2'-bipyridine, x = 8, **b**; 4,4'-dimethyl-2,2'-bipyridine, x = 8, **b**; 5,5'-dimethyl-2,2'-bipyridine, x = 8, **b**; 4,4'-di-*tert*-butyl-2,2'-bipyridine, x = 8, **b**; 3,4,7,8-tetramethyl-1,10-phenantroline, x = 6, **b**; 2,2'-bi(4,5-dihydrothiazine), x = 8, **b**; (R/S)-2-(1-hydroxyethyl)pyridine, x = 8, **b**), Ni₉Mo₆L_x (L = 2,2'-bipyridine, x = 8, **b**; 3,4,7,8-tetramethyl-1,10-phenantroline, x = 6, **b**), and Co₁Cu₈W₆(Me₃tacn)₈, **t** [12–20]. The formation of stable crystalline product depended strongly on L: M²⁺ molar ratio in solution. For the chelating ligands, the L:M²⁺ of 1:1 was sufficient to observe a complete or an almost complete capping of the peripheric M²⁺ sites, with the resulting L:M²⁺ ratio of 8:8 (prevalently), 7:8 or 6:8 in the cluster coverage (in the case of bis-chelating ligands), and 8:8 (in the case of tridentate Me₃tacn),

and 16:8, 14:8, or 12:8, and 24:8, respectively, counting separately each coordinated donor atom. For the linker-type ligands, the effective growth of the crystals was observed only by some excess of L, 1.5:1, 5:1, 7:1, or 20:1, with respect to the M^{2+} , to give the cluster coverage ratio L: M^{2+} between 12:8 and 4:8. In this work, for the first time, we have the opportunity to present compounds based on 15-centered clusters containing exclusively monodentate (without the bridging function) ligands, pyNO, and 4-phpyNO. To achieve effective crystallization, the use of a minimum of 30-fold excess of the ligand was required, with the resulting coverage L: M^{2+} ratio 12:8 (**1**) and 7:8 (10:7 ratio involving all 4-phpyNO in the crystal structure) (**2**) observed. Although no direct evidence was shown for the presence of complete 15-nuclear species in solution, the thermodynamic equilibria can be inferred to operate in solution, 15-nuclear cores acting as super-complexes with eight triple coordination sites located at the corners of super-cube sublattice. The above diversification in the ease of the crystal formation is in agreement with the thermodynamic prediction of complex stability considering the chelate effect, or “anchoring” due to the bridging, against the “simple” coordination of monodentate ligand. The ligand shell disorder in **1** and **2** is unprecedented along the entire family, and may be understood in terms of the degree of M–L bond rigidity and intercluster interactions inscribed in the ligand structure and M–L bonding mode. The longer linker ligands (e.g., 4,4'-bipyridine mono-*N*-oxide, 4,4'-bpmo; 4,4'-bipyridine di-*N*-oxide, 4,4'-bpdo) [16,17] form quite easily the bridging connections between clusters, and/or participate in the hydrogen bond supramolecular interaction network. On the other hand, the convergent bidentate ligand (frequently equipped with the remote substituents, e.g., 4,4'-dimethyl-2,2'-bipyridine, 4,4'-di-*tert*-butyl-2,2'-bipyridine, or 4,7-di-phenyl-1,10-phenantroline) [20] fill the intercluster space with the π – π synthons or van der Waals contacts. In both cases, the degree of freedom is strongly limited, which prevents the disorder. Interestingly, the dataset for pyrazine mono-*N*-oxide (pzmo) ligand [16], the shorter analog of 4,4'-bpmo, fairly resembles that of pyNO in **1**: (i) one of the pzmo ligands reveals severe positional disorder, and (ii) preparation of the product requires the ratio L: Co^{2+} ratio of 20:1, a little less than 30:1 in **1**. The occurrence of disorder in both cases may be correlated with the small volumes of both ligands, whereas the differences are definitely related to the natural preferences for intermolecular interactions. Coming to the compound **2**, the monodentate or crystallization form of 4-phpyNO moiety can be confronted with the diversity of coordination modes, bridging and monodentate, noted also both for $Co_9W_6(4,4'\text{-bpmo})_{4,6}$ and $Co_9W_6(4,4'\text{-bpdo})_{12}$.

2.2. Magnetic Properties

Temperature dependences of the molar magnetic susceptibility $\chi T(T)$ in the $T = 1.8$ – 300 K and $H_{dc} = 1$ kOe for **1** and **2** are presented in Figure 2. The room-temperature χT value for cyanide-bridged cluster of **1** and **2** is 26.57 and 29.58 $\text{cm}^3 \text{mol}^{-1} \text{K}$, respectively, which are in the range 26.25 – 33.00 expected for combined contribution of nine $^{HS}Co^{II}$ (with $S = 3/2$ and $g = 2.4$ – 2.7) and six W^V ions (with $S = 1/2$ and $g = 2.0$). The continuous increase of χT value to 100.50 and 95.49 $\text{cm}^3 \cdot \text{mol}^{-1} \cdot \text{K}$ at 10.25 and 7.58 K for **1** and **2**, respectively, indicates ferromagnetic superexchange interactions between ion centers connected by CN-bridges. After reaching the maximum value, the signal drops to 64.47 and 72.63 $\text{cm}^3 \cdot \text{mol}^{-1} \cdot \text{K}$ at 1.8 K for **1** and **2**, respectively, which is related to the intercluster interaction and zero-field splitting effect on $^{HS}Co^{II}$ ions. The maxima of χT correspond well to the theoretical value of 92.12 $\text{cm}^3 \text{mol}^{-1} \text{K}$ expected for isolated spins $S_{av} = 15/2$ with $g_{av} = 3.40$, when calculations with standard parameters for W^V ($S = 1/2$, $g = 2.0$) and effective spin approach for $^{LT}Co^{II}$ ($S = 1/2$, $g = 13/3$) are used. The insets in Figure 2 show isothermal field dependences of magnetization $M(H)$ in the magnetic field range $H_{dc} = 0$ – 70 kOe at 1.8 K to support the ferromagnetic type of interaction. Almost complete saturation is achieved with the values of 25.40 (**1**) and 25.47 (**2**) N_{β} at 70 kOe, which corresponds to the expected value of 25.5 μ_B calculated for $S = 15/2$ with $g = 3.4$. The above characteristics and related numbers are in line with previous observations along the family [13–17].

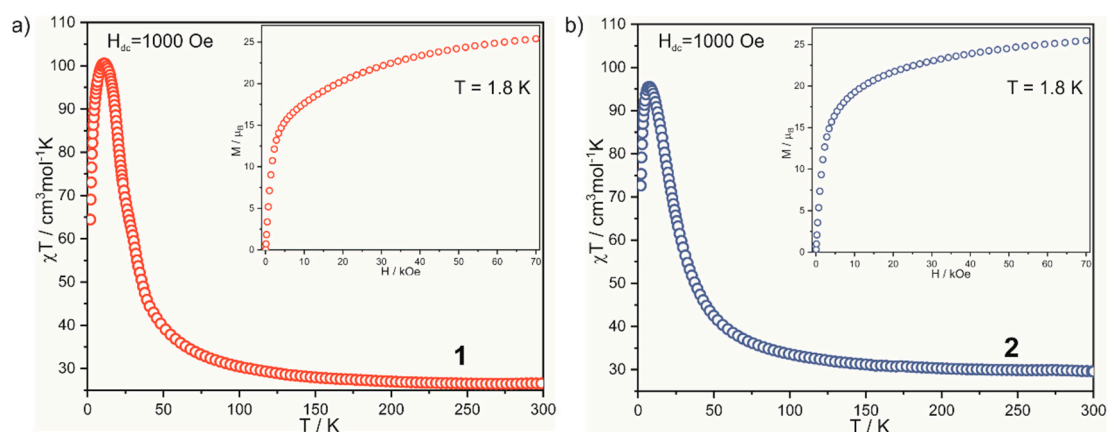


Figure 2. Temperature dependence of χT for **1** (a) and **2** (b) measured at $H = 1000$ Oe. Inset: isothermal magnetization at $T = 1.8$ K for both compounds, **1** (a) and **2** (b).

Unfortunately, no signature of slow magnetic relaxation was observed in zero or non-zero H_{dc} field and this can be related to the high symmetry of the coordination backbone (Figure S10, ESI†). Along with the twelve compounds shown previously, we have indicated that distinct characteristics with the $\chi''(T)$ maxima above $T = 1.8$ K could be observed only in the case of covering with 7,2,2'-bpdo or 24 MeOH. We explained their presence with the suitable magnetic anisotropy due to asymmetry of coverage and/or to significant deformation of the central Co moieties [16] described by SHAPE analysis. Considering **1** and **2**, the attempt of serendipitous induction of coverage asymmetry failed. Coming to the SHAPE analysis, rather highly symmetric central $[\text{Co}(\mu\text{-NC})_6]$ moieties was indicated in both compounds, either (Figure S11, Tables S6 and S7, ESI†). Some diversification was observed for the external Co units; however, this was not followed by the SMM behavior. Thus, the complete information set for the diverse fourteen compounds in this matter leads us to the conclusion that Co_9W_6 is rather difficult to functionalize toward outstanding SMM behavior, either by the ligand decoration or by the plausible accidental asymmetric truncation/extension of the coordination skeleton.

3. Experimental

3.1. Reagents and Materials

$\text{K}_4[\text{W}(\text{CN})_8]\cdot 2\text{H}_2\text{O}$ and $\text{TBA}_3[\text{W}^{\text{V}}(\text{CN})_8]$ were obtained according to the standard procedure. Firstly, $\text{K}_4[\text{W}^{\text{IV}}(\text{CN})_8]\cdot 2\text{H}_2\text{O}$ was obtained from K_2WO_4 via the combined reduction–cyanation–oxidation protocol involving NaBH_4 , perhydrol, and KCN in $\text{H}_2\text{O}/\text{CH}_3\text{COOH}$ media [21]. Then, $\text{K}_3[\text{W}^{\text{V}}(\text{CN})_8]$ was obtained through the oxidation of $\text{K}_4[\text{W}^{\text{IV}}(\text{CN})_8]$ in aqueous-acidic media (HNO_3), followed by immediate precipitation of $\text{Ag}_3[\text{W}^{\text{V}}(\text{CN})_8]$ using AgNO_3 . $\text{Na}_3[\text{W}^{\text{V}}(\text{CN})_8]\cdot 4\text{H}_2\text{O}$ was crystallized from the solution acquired after the solid-state solution metathesis between NaCl and $\text{Ag}_3[\text{W}^{\text{V}}(\text{CN})_8]_{(s)}$ in H_2O . Finally, $\text{TBA}_3[\text{W}^{\text{V}}(\text{CN})_8]$ was precipitated from the aqueous solution of $\text{Na}_3[\text{W}^{\text{V}}(\text{CN})_8]$ using TBACl . Inorganic substances were purchased from commercial sources (Sigma Aldrich, Poznań, Poland, Alfa Aesar, Kandel, Germany, Acros Organics, Poznań, Poland). Ligands pyridine *N*-oxide (pyNO, 95%) and 4-phenylpyridine *N*-oxide (4-phpyNO, 98%) were purchased from Sigma Aldrich and were used without further purification.

3.2. X-ray Diffraction Analysis

Single-crystal X-ray diffraction experiment of **1** and **2** was performed using Bruker D8 Quest Eco diffractometer equipped with Photon50 CMOS detector with standard Mo ($K\alpha$, $\lambda = 0.71073$ Å) radiation source, graphite monochromator, and Oxford Cryosystem cooling system. Measurements were performed at 100 K for crystals of **1** and **2**, covered by NVH immersion oil in order to prevent the exchange of crystallization solvent and structure degradation. The structures **1** and **2** were solved using

SHELXT and refined with full-matrix least-squares procedure on F^2 using SHELXL with Olex2 graphic interface. All non-hydrogen atoms were refined with anisotropic parameters. Positions of hydrogen atoms were assigned at the idealized positions using the riding model. Due to a large structural disorder on pyNO ligands in **1** and 4-phpyNO ligands in **2**, some restraints (DFIX, DANG, SIMU, DELU) on carbon or nitrogen atoms were applied. Relatively high residual density in the vicinity of some of the tungsten atoms is probably caused by an unaccounted disorder of cyanide groups. The results of data collection and structure refinement of **1** and **2** have been summarized in Table 1. CCDC reference numbers for the crystal structure are 1972361 (**1**) and 1972362 (**2**). Structural figures were prepared using the Mercury software. Powder X-ray diffraction data for **1** and **2** were collected using a Bruker D8 Advance Eco powder diffractometer equipped with Cu ($K\alpha$, $\lambda = 1.5419 \text{ \AA}$) radiation source. The measurements were conducted for polycrystalline samples in the mother solution inserted into a glass capillary (0.5 mm) [22,23].

3.3. Physical Techniques and Calculations

Elemental analyses of CHNS were performed on an Elemental Vario Micro Cube CHNS analyzer. The infrared absorption spectra were collected on the selected single crystals on an FT-IR Thermo Scientific Nicolet iN10 microscope. UV-Vis absorption spectra were collected on thin films of powder samples dispersed in NVH immersion oil using a Perkin-Elmer Lambda-35 spectrophotometer. The thermogravimetric (TGA) curves were collected for the polycrystalline samples using a Rigaku Thermo Plus TG8120 apparatus with aluminum pans as holders. The data were collected in the temperature range 20–375 °C under air atmosphere with a heating rate of 1 °C per minute. Magnetic data were collected using Quantum Design MPMS-3 Evercool magnetometer. The powder samples were measured in the glass tube covered by a small amount of the mother solution. Diamagnetic corrections from the sample, mother solution, and sample holder were introduced [24]. Continuous Shape Measure Analysis for the coordination sphere of each metal complex was performed using a SHAPE software [25].

3.4. Synthetic Procedures

Synthesis of 1. The 14.7 mg (0.06 mmol) of $\text{CoCl}_2 \cdot 6\text{H}_2\text{O}$ was dissolved together with 45 mg (0.04 mmol) of $\text{TBA}_3[\text{W}(\text{CN})_8]$ in 4 mL MeOH. The red solution was stirred for ca. 2 min, and the methanolic (2 mL) solution of 171.2 mg (1.8 mmol) of pyNO ligand was added. The deep-red solution was mixed for another 2 min, filtrated off, and tightly closed. After one day, dark red crystals of **1** appeared. The composition of $\{\text{Co}^{\text{II}}[\text{Co}^{\text{II}}_8(\text{pyNO})_{12}(\text{MeOH})_{12}][\text{W}^{\text{V}}(\text{CN})_8]_6\}$ was defined by a single-crystal X-ray diffraction analysis. Phase purity was proved by XRD data. Crystals are stable in mother solution; however, solvent molecules are exchanged for water molecules in air. The formula of the hydrated form $\{\text{Co}^{\text{II}}_9[\text{W}^{\text{V}}(\text{CN})_8]_6(\text{pyNO})_{12} \cdot 1\text{MeOH} \cdot 17\text{H}_2\text{O}\}$ (**1**^{hyd}) was determined by CHN elemental analysis and TGA measurement. Yield for **1**^{hyd}: 41% (based on Co). Elemental analysis. Calc. for $\text{C}_{109}\text{H}_{98}\text{Co}_9\text{N}_{60}\text{O}_{30}\text{W}_6$: C, 30.01%; H, 2.26%; N, 19.27%. Found: C, 30.23%; H, 2.41%; N, 19.05%. **1**^{hyd} was of poor crystallinity, which precluded reliable crystal structure determination. IR spectrum for **1**. Cyanide stretching vibrations $\nu(\text{C}\equiv\text{N})$ at 2213, 2172, and 2144 cm^{-1} are related to both bridging and terminal cyanides in $[\text{W}^{\text{V}}(\text{CN})_8]^{3-}$ building blocks. UV-Vis spectrum for **1**. The wide range of absorption bands (UV–750 cm^{-1}) can be explained by the sum of ligand field electronic transitions of $[\text{W}^{\text{V}}(\text{CN})_8]^{3-}$ ions, d–d electronic transitions of $^{\text{HS}}\text{Co}^{\text{II}}$ ion, and metal-to-metal charge transfer (MMCT) electronic transitions.

Synthesis of 2. The 14.7 mg (0.06 mmol) of $\text{CoCl}_2 \cdot 6\text{H}_2\text{O}$ was dissolved together with 45 mg (0.04 mmol) of $\text{TBA}_3[\text{W}(\text{CN})_8]$ in 4 mL MeOH. The red solution was stirred for ca. 2 min, and the methanolic (2 mL) solution of 308.2 mg (1.8 mmol) of 4-phpyNO ligand was added. The blood-red solution was mixed for another 2 min, filtrated off, and tightly closed. After one day, dark red crystals of **2** appeared. The composition of $\{\text{Co}^{\text{II}}[\text{Co}^{\text{II}}_8(4\text{-phpyNO})_7(\text{MeOH})_{17}][\text{W}^{\text{V}}(\text{CN})_8]_6\} \cdot 7\text{MeOH} \cdot (4\text{-phpyNO})_3$ was defined

by a single-crystal X-ray diffraction analysis. Phase purity was proved by XRD data. Crystals are stable in mother solution; however, solvent molecules are exchanged for water molecules in air. The formula of the hydrated form $\{\text{Co}^{\text{II}}_9[\text{W}^{\text{V}}(\text{CN})_8]_6(4\text{-phpyNO})_{10}\cdot 1\text{MeOH}\cdot 17\text{H}_2\text{O}\}$ (2^{hyd}) was determined by CHN elemental analysis and TGA measurement. Yield for 2^{hyd} : 37% (based on Co). Elemental anal. calc. for $\text{C}_{159}\text{H}_{128}\text{Co}_9\text{N}_{58}\text{O}_{29}\text{W}_6$: C, 38.59%; H, 2.61%; N, 16.42%. Found: C, 38.78%; H, 2.85%; N, 16.68%. 2^{hyd} was of poor crystallinity, which precluded reliable crystal structure determination. IR spectrum for **2**. Cyanide stretching vibrations $\nu(\text{C}\equiv\text{N})$ at 2220, 2174, and 2150 cm^{-1} are related to both bridging and terminal cyanides in $[\text{W}^{\text{V}}(\text{CN})_8]^{3-}$ building blocks. UV–Vis spectrum for **2**. The wide range of absorption bands (UV— 750 cm^{-1}) can be explained by the sum of ligand field electronic transitions of $[\text{W}^{\text{V}}(\text{CN})_8]^{3-}$ ions, d–d electronic transitions of $^{\text{HS}}\text{Co}^{\text{II}}$ ion, and metal-to-metal charge transfer (MMCT) electronic transitions.

Comment: It is necessary to add that only a drastic excess of ligand relative to Co^{2+} ions, here 45:1, caused the equilibrium shift toward the crystallization of the product; a change of the ligand/ Co^{2+} ratio results in a reduction of yield and product quality or prevents its formation.

4. Conclusions

We have presented two new pentadecanuclear cluster-based compounds: $\{\text{Co}^{\text{II}}[\text{Co}^{\text{II}}_8(\text{pyNO})_{12}(\text{MeOH})_{12}][\text{W}^{\text{V}}(\text{CN})_8]_6\}$ (**1**) and $\{\text{Co}^{\text{II}}[\text{Co}^{\text{II}}_8(4\text{-phpyNO})_7(\text{MeOH})_{17}][\text{W}^{\text{V}}(\text{CN})_8]_6\cdot 7\text{MeOH}\cdot (4\text{-phpyNO})_3\}$ (**2**), obtained in crystalline form through a suitable combination of Co^{2+} and $[\text{W}(\text{CN})_8]^{3-}$ ions and monodentate pyNO or 4-phpyNO ligands. Their crystal structure and magnetic properties were examined. PyNO ligands decorating the cluster core in **1** form densely packed π – π supramolecular structure, in which the symmetrical surrounding of the clusters is observed. In addition, parallel π – π interaction between ligands coordinated to the same ion center is observed, which has not been seen in $\text{M}_9\text{M}'_6$ clusters with monodentate ligand-based yet. In compound **2**, the 4-phpyNO ligands either decorate the M sites or act as the crystallization molecules. In both structures, a significant ligand shell structural disorder was observed, with the partial occupancy of individual coordinating units (ligands, solvents) of 0.25, 0.50, or 0.75 determined within the solution and refinement model. DC magnetic properties indicate the high-spin ground state due to ferromagnetic Co(II)–W(V) interactions, in agreement with the previous reported Co_9W_6 cluster-based compounds. Due to the high symmetrical arrangement of clusters in **1** zero-signal in ac measurements was observed. In **2**, 4-phpyNO longer than pyNO offers more degrees of freedom due to the phenyl ring rotation but it turns out to be insufficient to observe $\chi''(\text{T})$ signal. However, the presented supramolecular building blocks $\text{Co}_9\text{W}_6\text{L}_x$ can be perceived as a potential source of polynuclear nanometer scale building block for the π – π supramolecular organization of supramolecular networks. The research is underway in the project group.

Going beyond the above Co_9W_6 -L approach, the magnetic properties can be modified by the topological changes done to six capped body-centered cube topology through the modification of other synthetic conditions. For example, the slow diffusion CoCl_2 , RbCl , and $\text{Rb}_3[\text{W}(\text{CN})_8]$ in water-acetone media leads to the porous-like $\text{Co}_7[\text{W}(\text{CN})_8]_4\text{Cl}_2\cdot 29\text{H}_2\text{O}$ 3D network with 1.4 nm inter-skeletal diameter, containing the tubular wires $\{\text{Co}_5\text{W}_4\}$ that could be perceived as the in situ-formed 1D secondary building units (SBU) [26]. The long-range magnetic ordering (LRMO) temperature $T_C = 29\text{ K}$ and coercive field $H_c = 5.5\text{ kOe}$ were found. Very similar thick wire 1D arrangement with T_N of 3.5 K has been acquired via the unique direct quadruple bridging between Mn_9W_6 clusters, assisted by the bridging of dpe linkers [27]. The slow diffusion of water vapor into the mixture of Mn_9W_6 and pyrazine-*N,N*-dioxide (pzdo) in MeOH leads to the 2D topology closely related to the cluster surface grid, not achieved in the typical aqueous conditions used for the extended $[\text{M}(\text{CN})_8]^{n-}$ networks [28]. The above observations still allow to reasonably consider the acquisition of the large defected discrete $\text{Co}_x\text{W}_y^{n+/-}$ species or single chains based on such motifs, potentially hosting the slow magnetic relaxation properties. Finally, the use of the triazacyclononane (tacn) family allows to afford 15-nuclear and larger related 20-nuclear topologies, which offer the stabilization of paramagnetic $[\text{W}(\text{CN})_8]^{3-}$

anions, [19,29,30] spin-crossover on all nine Fe(II) sites [31], and photomagnetic properties in the case of $\text{Cu}^{\text{II}}\text{-}[\text{Mo}^{\text{IV}}(\text{CN})_8]^{4-}$ species [32].

Supplementary Materials: The following are available online. Figure S1 (IR spectra), Figure S2 (TGA curves), Figure S3 (UV-Vis-NIR absorption spectra), Figures S4 and S5 (Crystal structure illustrations), Figure S6 (Stacking interactions), Figure S7 and Table S8 (Crystal packing), Figure S9 (PXRD patterns), Figure S10 (out-of-phase ac magnetic measurements), Figure S11 (SHAPE maps for Co(II) centers), Table S1 and Table S2 (detailed structural parameters of 3d metal complexes), Table S2 (detailed structural parameters of 3d metal complexes in 2), Table S3 and Table S4 (CSM analysis), Table S5 (H-bonds parameters), Tables S6 and S7 (the overview of the structural parameters).

Author Contributions: The manuscript was written through contributions of all authors. All authors have given approval to the final version of the manuscript. They specifically contributed as follows: M.L. has performed the syntheses and basic characterization of substrates and compounds, and participated in structural and magnetic measurements and analyses. J.K. led the structural and magnetic measurements, and performed the relevant data analysis. R.P. has appointed the research topic and supervised the whole research work. All authors have read and agreed to the published version of the manuscript.

Funding: This research was funded by the Polish National Science Centre within the SONATA BIS 4 Project UMO-2014/14/E/ST5/00357. European Regional Development Fund in the framework of the Polish Innovation Economy Operational Program (contract no. POIG.02.01.00-12023/08). Magnetic measurements were performed using the equipment purchased from the Large Research Infrastructure Fund of the Polish Ministry of Science and Higher Education (decision no. 6350/IA/158/2013.1).

Conflicts of Interest: The authors declare no conflict of interest.

References

1. Dong, D.-P.; Liu, T.; Kanegawa, S.; Kang, S.; Sato, O.; He, C.; Duan, C.-Y. Photoswitchable dynamic magnetic relaxation in a well-isolated $\{\text{Fe}_2\text{Co}\}$ double-zigzag chain. *Angew. Chem. Int. Ed.* **2012**, *51*, 5119–5123. [[CrossRef](#)]
2. Mondal, A.; Chamoreau, L.M.; Li, Y.; Journaux, Y.; Seuleiman, M.; Lescouëzec, R. W-Co discrete complex exhibiting photo- and thermo-induced magnetisation. *Chem. Eur. J.* **2013**, *19*, 7682–7685. [[CrossRef](#)]
3. Daffé, N.; Jiménez, J.R.; Studniarek, M.; Benchohra, A.; Arrio, M.A.; Lescouëzec, R.; Dreiser, J. Direct observation of charge transfer and magnetism in Fe_4Co_4 cyanide-bridged molecular cubes. *J. Phys. Chem. Lett.* **2019**, *10*, 1799–1804. [[CrossRef](#)] [[PubMed](#)]
4. Zhang, Y.Z.; Dolinar, B.S.; Liu, S.; Brown, A.J.; Zhang, X.; Wang, Z.X.; Dunbar, K.R. Enforcing Ising-like magnetic anisotropy via trigonal distortion in the design of a W(V)-Co(II) cyanide single-chain magnet. *Chem. Sci.* **2018**, *9*, 119–124. [[CrossRef](#)] [[PubMed](#)]
5. Chorazy, S.; Nakabayashi, K.; Imoto, K.; Mlynarski, J.; Sieklucka, B.; Ohkoshi, S. Conjunction of chirality and slow magnetic relaxation in the supramolecular network constructed of crossed cyano-bridged $\text{Co}^{\text{II}}\text{-W}^{\text{V}}$ molecular chains. *J. Am. Chem. Soc.* **2012**, *134*, 16151–16154. [[CrossRef](#)] [[PubMed](#)]
6. Wei, R.M.; Cao, F.; Li, J.; Yang, L.; Han, Y.; Zhang, X.L.; Wang, X.Y.; Song, Y. Single-chain magnets based on octacyanotungstate with the highest energy barriers for cyanide compounds. *Sci. Rep.* **2016**, *6*, 24372. [[CrossRef](#)]
7. Pichon, C.; Suaud, N.; Duhayon, C.; Guihery, N.; Sutter, J.P. Cyano-bridged Fe(II)-Cr(III) single-chain magnet based on pentagonal bipyramid units: On the added value of aligned axial anisotropy. *J. Am. Chem. Soc.* **2018**, *140*, 7698–7704. [[CrossRef](#)]
8. Venkatakrishnan, T.S.; Sahoo, S.; Brefuel, N.; Duhayon, C.; Paulsen, C.; Barra, A.L.; Ramasesha, S.; Sutter, J.P. Enhanced ion anisotropy by nonconventional coordination geometry: Single-chain magnet behavior for a $[\{\text{Fe}^{\text{II}}\text{L}\}_2\{\text{Nb}^{\text{IV}}(\text{CN})_8\}]$ helical chain compound designed with heptacoordinate Fe^{II} . *J. Am. Chem. Soc.* **2010**, *132*, 6047–6056. [[CrossRef](#)]
9. Pinkowicz, D.; Southerland, H.I.; Avendano, C.; Prosvirin, A.; Sanders, C.; Wernsdorfer, W.; Pedersen, K.S.; Dreiser, J.; Clerac, R.; Nehr Korn, J.; et al. Cyanide single-molecule magnets exhibiting solvent dependent reversible “on” and “off” exchange bias behavior. *J. Am. Chem. Soc.* **2015**, *137*, 14406–14422. [[CrossRef](#)]
10. Visinescu, D.; Alexandru, M.G.; Madalan, A.M.; Pichon, C.; Duhayon, C.; Sutter, J.P.; Andruh, M. Magneto-structural variety of new 3d-4f-4 (5) d heterotrimetallic complexes. *Dalton Trans.* **2015**, *44*, 16713–16727. [[CrossRef](#)]

11. Kumar, K.; Stefańczyk, O.; Chorazy, S.; Nakabayashi, K.; Sieklucka, B.; Ohkoshi, S. Effect of noble metals on luminescence and single-molecule magnet behavior in the cyanido-bridged Ln–Ag and Ln–Au (Ln = Dy, Yb, Er) complexes. *Inorg. Chem.* **2019**, *58*, 5677–5687. [[CrossRef](#)] [[PubMed](#)]
12. Song, Y.; Zhang, P.; Ren, X.M.; Shen, X.F.; Li, Y.Z.; You, X.Z. Octacyanometallate-based single-molecule magnets: $\text{Co}^{\text{II}}\text{W}^{\text{V6}}$ (M = W, Mo). *J. Am. Chem. Soc.* **2005**, *127*, 3708–3709. [[CrossRef](#)] [[PubMed](#)]
13. Chorazy, S.; Hoczek, A.; Kubicki, M.; Tokoro, H.; Ohkoshi, S.; Sieklucka, B.; Podgajny, R. The solvent effect on the structural and magnetic features of bidentate ligand-capped $\{\text{Co}^{\text{II}}_9[\text{W}^{\text{V}}(\text{CN})_8]_6\}$ single-molecule magnets. *Cryst. Eng. Comm.* **2016**, *18*, 1495–1504. [[CrossRef](#)]
14. Chorazy, S.; Rams, M.; Hoczek, A.; Czarnecki, B.; Sieklucka, B.; Ohkoshi, S.; Podgajny, R. Structural anisotropy of cyanido-bridged $\{\text{Co}^{\text{II}}_9\text{W}^{\text{V6}}\}$ single-molecule magnets induced by bidentate ligands: Towards the rational enhancement of an energy barrier. *Chem. Commun.* **2016**, *52*, 4772–4775. [[CrossRef](#)]
15. Chorazy, S.; Reczyński, M.; Podgajny, R.; Nogas, W.; Buda, S.; Rams, M.; Nitek, W.; Nowicka, B.; Mlynarski, J.; Ohkoshi, S.; et al. Implementation of chirality into high-spin ferromagnetic $\text{Co}^{\text{II}}\text{W}^{\text{V6}}$ and $\text{Ni}^{\text{II}}\text{W}^{\text{V6}}$ cyanido-bridged clusters. *Cryst. Growth Des.* **2015**, *15*, 3573–3581. [[CrossRef](#)]
16. Kobylarczyk, J.; Augustyniak, K.; Chorazy, S.; Nowicka, B.; Pinkowicz, D.; Koziel, M.; Muziol, T.; Podgajny, R. Cyanido-bridged clusters with remote N-oxide groups for branched multimetallic systems. *Cryst. Growth Des.* **2018**, *18*, 4766–4776. [[CrossRef](#)]
17. Chorazy, S.; Podgajny, R.; Nitek, W.; Rams, M.; Ohkoshi, S.; Sieklucka, B. Supramolecular chains and coordination nanowires constructed of high-spin $\text{Co}^{\text{II}}\text{W}^{\text{V6}}$ clusters and 4,4'-bpdo linkers. *Cryst. Growth Des.* **2013**, *13*, 3036–3045. [[CrossRef](#)]
18. Pinkowicz, D.; Podgajny, R.; Nowicka, B.; Chorazy, S.; Reczynski, M.; Sieklucka, B. Magnetic clusters based on octacyanidometallates. *Inorg. Chem. Front.* **2015**, *2*, 10–27. [[CrossRef](#)]
19. Liberka, M.; Kobylarczyk, J.; Muziol, T.M.; Ohkoshi, S.; Chorazy, S.; Podgajny, R. A heterotrimetallic synthetic approach in versatile functionalization of nanosized $\{\text{M}_x\text{Cu}_{13-x}\text{W}_7\}^{3+}$ and $\{\text{M}_1\text{Cu}_8\text{W}_6\}$ (M = Co, Ni, Mn, Fe) metal–Cyanide magnetic clusters. *Inorg. Chem. Front.* **2019**, *6*, 3104–3118. [[CrossRef](#)]
20. Kobylarczyk, J.; Liberka, M.; Konieczny, P.; Baran, S.; Kubicki, M.; Korzeniak, T.; Podgajny, R. Bulky ligands shape the separation between the large spin carriers to condition field-induced slow magnetic relaxation. *Dalton Trans.* **2020**, *49*, 300–311. [[CrossRef](#)]
21. Szklarzewicz, J.; Matoga, D.; Lewiński, K. Photocatalytical decomposition of hydrazine in $\text{K}_4[\text{Mo}(\text{CN})_8]$ solution: X-ray crystal structure of $(\text{PPh}_4)_2[\text{Mo}(\text{CN})_4\text{O}(\text{NH}_3)] \cdot 2\text{H}_2\text{O}$. *Inorg. Chim. Acta* **2007**, *360*, 2002–2008. [[CrossRef](#)]
22. Sheldrick, G.M. A short history of SHELX. *Acta Crystallogr. Sect. A* **2008**, *64*, 112–122. [[CrossRef](#)] [[PubMed](#)]
23. Macrae, C.F.; Bruno, I.J.; Chisholm, J.A.; Edgington, P.R.; McCabe, P.; Pidcock, E.; Rodriguez-Monge, L.; Taylor, R.; van de Streek, J.; Wood, P.A. Mercury CSD 2.0—new features for the visualization and investigation of crystal structures. *J. Appl. Crystallogr.* **2008**, *41*, 466–470. [[CrossRef](#)]
24. Bain, G.A.; Berry, J.F. Dimagnetic corrections and pascal's constants. *J. Chem. Educ.* **2008**, *85*, 532. [[CrossRef](#)]
25. Llunell, M.; Casanova, D.; Cirera, J.; Bofill, J.; Alemany, P.; Alvarez, S.; Pinsky, M.; Avnir, D. *SHAPE v. 2.1. Program. for the Calculation of Continuous Shape Measures of Polygonal and Polyhedral Molecular Fragments*; University of Barcelona: Barcelona, Spain, 2013.
26. Nakabayashi, K.; Chorazy, S.; Komine, M.; Miyamoto, Y.; Takahashi, D.; Sieklucka, B.; Ohkoshi, S. Magnetic Lotus root based on a cyanido-bridged Co–W metal assembly. *Cryst. Growth Des.* **2017**, *17*, 4511–4515. [[CrossRef](#)]
27. Podgajny, R.; Chorazy, S.; Nitek, W.; Rams, M.; Balanda, M.; Sieklucka, B. $\{\text{Mn}^{\text{II}}\text{W}^{\text{V6}}\}_n$ Nanowires Organized into Three-Dimensional Hybrid Network of I^1O^2 Topology. *Cryst. Growth Des.* **2010**, *10*, 4693–4696. [[CrossRef](#)]
28. Podgajny, R.; Pinkowicz, D.; Czarnecki, B.; Koziel, M.; Chorazy, S.; Wis, M.; Nitek, W.; Rams, M.; Sieklucka, B. Role of Pyrazine-*N,N'*-dioxide in $[\text{W}(\text{CN})_8]^{n-}$ -Based Hybrid Networks: Anion– π Interactions. *Cryst. Growth Des.* **2014**, *14*, 4030–4040. [[CrossRef](#)]
29. Wang, J.; Zhang, Z.C.; Wang, H.S.; Kang, L.C.; Zhou, H.B.; Song, Y.; You, X.Z. Eicosanuclear cluster $[\text{Cu}_{13}\text{W}_7]$ of copper-octacyanotungstate bimetallic assembly: Synthesis, Structure, and magnetic properties. *Inorg. Chem.* **2010**, *49*, 3101–3103. [[CrossRef](#)]

30. Zhang, Z.; Liu, Y.; Wei, R.M.; Sheng, Z.H.; Wang, P.; Song, Y. electrochemical synthesis and magnetic properties of $[\text{Cu}_9\text{W}_6]$: The ultimate member of the quindecannuclear octacyanometallate-based transition-metal cluster? *Inorg. Chem.* **2015**, *54*, 11049–11051. [[CrossRef](#)]
31. Chorazy, S.; Stanek, J.J.; Kobylarczyk, J.; Ohkoshi, S.; Sieklucka, B.; Podgajny, R. Modulation of the Fe^{II} spin crossover effect in the pentadecannuclear $\{\text{Fe}_9[\text{M}(\text{CN})_8]_6\}$ ($\text{M} = \text{Re}, \text{W}$) clusters by facial coordination of tridentate polyamine ligands. *Dalton Trans.* **2017**, *46*, 8027–8036. [[CrossRef](#)]
32. Bridonneau, N.; Chamoreau, L.M.; Gontard, G.; Cantin, J.L.; von Bardeleben, J.; Marvaud, V. A high-nuclearity metal-cyanide cluster $[\text{Mo}_6\text{Cu}_{14}]$ with photomagnetic properties. *Dalton Trans.* **2016**, *45*, 9412–9418. [[CrossRef](#)] [[PubMed](#)]

Sample Availability: Samples of the compounds **1** and **2** are available from the authors.



© 2020 by the authors. Licensee MDPI, Basel, Switzerland. This article is an open access article distributed under the terms and conditions of the Creative Commons Attribution (CC BY) license (<http://creativecommons.org/licenses/by/4.0/>).